THE JOURNAL OF PHYSICAL CHEMISTRY A
A JOURNAL OF THE AMERICAN CHEMICAL SOCIETY

pubs.acs.org/JPCA

Article

Molecular Hydrogen Acts as a Hydrogen Bond Proton Acceptor: From Protonated Betaine Tagging to the Weakest Hydrogen Bond

Blagoj Achevski and Ljupcho Pejov*

Cite This: *J. Phys. Chem. A* 2024, 128, 3968−3981

Read Online

ACCESS | Metrics & More | Article Recommendations | Supporting Information

ABSTRACT: In an attempt to gain further insights into the intermolecular interactions implied by Rizzo's group's cautionary tale related to molecular tagging in infrared multiple photon dissociation (IRMPD) spectroscopy with molecular messengers [Masson, A. et al.. *J. Chem. Phys.* **2015**, *143*, 104313], in the present study, we provide an in-depth analysis of the noncovalent interaction between the molecular hydrogen and protonated betaine molecule in the gas phase. We aim to shed some new light on the fundamental issues concerning the wide diapason of hydrogen-bonding-type intermolecular interactions, with a wide variety of proton acceptors. We demonstrate that in the course of tagging the protonated betaine with molecular hydrogen from the OH group side, it is the σ bond of molecular hydrogen that plays the role of hydrogen-bonding proton acceptor. The tagging thus induces a small yet significant red shift of the protonated betaine O−H stretching mode. We investigate the performance of a wide range of density functional theory (DFT) functionals for the calculation of anharmonic vibrational frequency shifts of the studied system, which are essential for the correct interpretation of the experimental IRMPD data. For an accurate prediction of the OH stretching frequency shifts, specifically designed functionals such as Handy's group HCTH/407 should be applied. The empirical dispersion correction enhances the systematic overestimation of the anharmonic frequency shift, characteristic of the most widely used DFT functionals. Combining the full-wave function approach with the charge field perturbation and natural bond orbital (NBO) deletion analyses, we demonstrate that the frequency shift in the OH-tagged structure is governed by the $\sigma_{HH} \rightarrow \sigma^*_{OH}$ intermolecular charge transfer. This interaction stabilizes the OH-tagged dimer as well, in contrast to the dipole−quadrupole electrostatic interaction energy term. Topological analysis of the electron density reveals the presence of an intermolecular bond critical point with a positive value of the density Laplacian very close to the lower limit for hydrogen bonds. NCI analyses demonstrate that the OH···H_2 interaction is weaker than the intramolecular CH···O one within the protonated betaine molecule, with the through of reduced density gradient appearing at less negative sign(λ_2)·ρ values. Analyzing the O−H stretching vibrational potential with the second-generation absolutely localized molecular orbitals energy decomposition analysis (ALMO-EDA 2) revealed that in the case of betaineH(+) tagged from the OH group side, the permanent electrostatics (ΔE_{elec}), polarization (ΔE_{pol}), and charge-transfer (ΔE_{ct}) contributions to the total intermolecular interaction energy contribute favorably to the weak hydrogen bond formation and to the red shift of the fundamental O−H stretching frequency, the ΔE_{ct} contribution being the most significant in the last context. The Pauli repulsion term, on the other hand, favors an O−H stretching frequency blue shift as a consequence of the vibrational confinement effects.

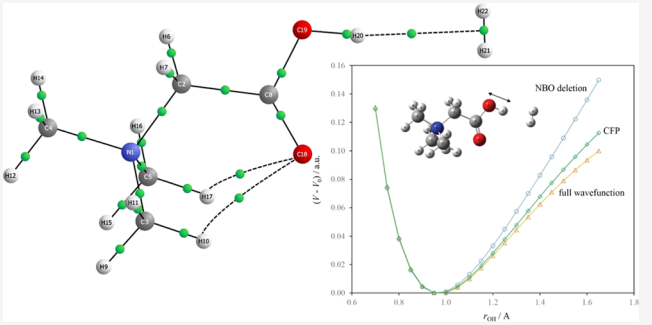

1. INTRODUCTION

Understanding the gas-phase structure and dynamics of biomolecular species is the first step toward better insights into their inclusion in more complex, biologically relevant media. The advent of infrared multiple photon dissociation (IRMPD) spectroscopic techniques has enabled numerous size-selected species to be explored in detail.[1] In this technique, a molecular ion is first mass-selected, trapped in either a Penning or radiofrequency trap, and subsequently irradiated with tunable infrared laser radiation. Once the laser frequency is resonant with an intramolecular vibrational mode of the ion, the corresponding IR photons are absorbed, which leads to their heating and subsequent fragmentation. A mass spectrometer is used to detect the fragment ions, serving as photon absorption indicators.

The IR action spectrum can thus be obtained if one follows the dependence of the extent of fragmentation on the laser wavelength. Alternatively, the IR action spectra can be

Received: February 29, 2024
Revised: April 22, 2024
Accepted: April 24, 2024
Published: May 9, 2024

https://doi.org/10.1021/acs.jpca.4c01331
J. Phys. Chem. A 2024, 128, 3968−3981

obtained by a combination of UV and IR lasers. The UV laser is initially used to cause ion fragmentation, provided that the particular ion has an appropriate chromophore. Taking the scan of the IR laser over a given vibrational band causes absorption of the radiation and subsequent reduction of the ground state population and consequent decrease of the fragmentation signal induced by UV irradiation.

In general, the number of absorbed photons that will eventually lead to ion fragmentation depends on numerous factors, such as the photon energy, the dissociation barrier, the initial temperature of the ion, etc. In the case of weakly bound clusters with small dissociation energies, cold ions can be dissociated upon absorption of even a single IR photon. Such a method is usually applied employing a weakly bound so-called "molecular messenger" to "tag" the investigated ion in a molecular beam or in an ion trap. H_2, He, Ne, and Ar are all typical examples of tags that attach to ions at very low temperatures and that can be detached upon absorption of one or more IR photons.[1] Such a photodissociation technique, demonstrated for the first time by Okumura et al.,[2,3] has been applied to numerous ionic species. Aside from the obvious advantages of this method, there is also an implicit assumption that the tagging species should not actually cause significant perturbation of the ion of interest. For example, Ne and Ar are known to cause quite large perturbations of the vibrational spectra of the investigated ions as a consequence of their large polarizabilities. Molecular hydrogen, on the other hand, was first thought to cause only minor perturbations, as demonstrated in the studies of protonated dipeptides, dicarboxylate anions, etc.[4−6] A recent study of protonated glycine and betaine by the group of Rizzo, however, seemed to have demonstrated quite the opposite.[7] Tagging with even a single H_2 molecule appeared to significantly affect some of the vibrational modes of these species.

Results from the experimental spectroscopic observations, however, lead only to differences in the vibrational eigenstates, not revealing their exact origin. Most of the band assignments, therefore, are usually based on empirical arguments and on "chemical intuition." As a consequence of this, any serious attempt to provide an in-depth understanding of molecular force fields should be based on sound theoretical analysis and argumentation.

Most of the simple and straightforward approaches toward this aim, which are automated in the available quantum mechanical computational codes, are based on algorithms involving the double-harmonic normal mode approximation and are being used often in conjunction with a density functional theory (DFT)-based method. While the harmonic approximation may suffice for many of the intramolecular modes, this is not the case with the modes involving stretching vibrations of the X-H fragments. There is firm evidence that systematic errors inherent to widely used DFT methods may cancel out with those due to the harmonic approximation, thus hampering any possibility to get a deeper insight into the nature of the molecular vibrational force field.[8,9]

Therefore, any rigorous calculation aiming to clarify the experimental observations and, at the same time, give correct insight into the factors determining the vibrational frequency shift of a particular mode of interest must be based on anharmonic treatment of the oscillators in question. This is particularly true for X-H oscillators due to the small mass of the H atom and, consequently, the relatively high vibrational amplitudes spanning a significant segment of the notably anharmonic part of the vibrational potential. Though theoretical approaches have been established for this purpose, such as the vibrational self-consistent field methods[10−13] and the perturbation theoretic approach by Barone,[14] these are computationally rather demanding and expensive, so that having a simpler yet rigorous theoretical approach for this purpose is highly desirable. We therefore developed and implemented the approach described further in the text.

In the present study, we aim to provide an in-depth theoretical understanding of the tagging of protonated betaine with H_2 in the gas phase. To avoid any ambiguities in the data interpretation of more complex systems, such as, e.g., the protonated glycine and other amino acids and peptides, it is rather useful to consider the tagging of protonated glycine's analogue in which all amine group hydrogen atoms have been replaced with methyl groups—betaine.[7] We go beyond the harmonic approximation to accurately calculate anharmonic vibrational frequencies and frequency shifts for the title system, which will be directly comparable to the experimental data. By providing an in-depth analysis of the performance of different density functionals in this context, we point out at certain systematic deficiencies thereof and at the overall effect of including dispersion, as well as long-range corrections to the existing functionals which are in wide use. The problem has been tackled, and it has been recognized that there is indeed a systematic deficiency in the more standard density functionals concerning this issue,[8,9,15] but no deeper theoretical insights have been provided.

At the same time, the basic driving forces that govern the mechanism of tagging the protonated betaine by molecular hydrogen seem to be not sufficiently understood. Though, at first sight, one may assume that polarization of molecular hydrogen by the charged betaineH(+) could provide conditions under which the dipole-induced dipole terms would be responsible for the overall stabilization of the dimer. The dipole−quadrupole and quadrupole−quadrupole interactions are potential candidates for stabilization too. However, the question as to whether the bonding between protonated betaine and H_2 is of purely electrostatic nature or if there is another physical mechanism that governs the association process has not been addressed. A tempting feature of the manifestation of this dimer's formation is the slight but non-negligible frequency red shift of the band corresponding to the fundamental $|0\rangle \rightarrow |1\rangle$ transition of the O−H stretching vibrational chromophore positioned on the betaineH(+) subunit. This feature has been the subject of the cautionary tale addressed by Rizzo and collaborators in their experimental IRMPD study of this system.[7] The tagging by molecular hydrogen might not be prone to altering the vibrational force field of the tagged unit. In the present study, we provide an in-depth theoretical analysis of the electron density of the possible tagged structures of the protonated betaine (betaineH(+)) by molecular hydrogen using Bader's analysis,[16] natural bond orbital (NBO),[17,18] and NCI analysis.[19] We also analyze the O−H stretching vibrational potential within the NBO deletion analysis, the charge field perturbation (CFP) approach,[20] as well as with the second-generation absolutely localized molecular orbitals energy decomposition analysis.[21,22] These analyses, which provided in-depth insights into the main forces governing the vibrational frequency shifts upon this noncovalent interaction, have allowed us to conclude that molecular hydrogen can act as a hydrogen-bonding proton acceptor. Thus, the situation when protonated betaine is

https://doi.org/10.1021/acs.jpca.4c01331
J. Phys. Chem. A 2024, 128, 3968−3981

tagged from the OH group side, with the proton pointing out at the center of the H−H σ-bond electron density, corresponds to one of the weakest hydrogen-bonding interactions (i.e., probably the weakest one) that have been described in the literature so far.

2. THEORETICAL METHODOLOGY AND COMPUTATIONAL DETAILS

2.1. General Computational Methodology. The potential energy surfaces (PESs) of free protonated betaine (further on denoted as betaineH(+)) as well as of betaineH(+) complex with a single H_2 molecule were thoroughly explored at several levels of theory using Schlegel's gradient optimization algorithm.[23] Aside from the standard PESs, we also explored the counterpoise-corrected PESs at some of the theoretical levels. The counterpoise correction was accounted for in each optimization step by the method of Boys−Bernardi.[24]

The employed levels of theory included the DFT methods based on the following combination of exchange and correlation functionals with or without inclusion of the dispersion corrections: B3LYP[25,26] and its long-range-corrected version using the method of Coulomb-attenuation (CAM-B3LYP[27]), the dispersion-corrected version of these two functionals with the D3 version of Grimme's correction with the Becke−Johnson damping[28] (B3LYP-GD3BJ and CAM-B3LYP-GD3BJ). Also, we have considered the LC-wHPBE long-range-corrected functional[29] as another example of this class (along with the CAM-B3LYP), which is actually the recommended variant of the LC-ωPBE functional,[30] and the Handy's group HCTH/407 gradient-corrected functional,[31,32] which has been specifically designed for noncovalent intermolecular interactions. Our intention was to carefully follow the influence of different aspects of the characteristics of the exchange and correlation functionals on the calculated parameters. Along with the DFT methods, in our study, we have also employed the double-hybrid methods, combining the exact HF exchange with an MP2-like correlation to the DFT part. These were the B2PLYP method,[33] along with its variant, including the empirical dispersion correction (B2PLYP-D[34]) and the B2PLYP method in combination with the D3 version of Grimme's correction with the Becke−Johnson damping[35,36] (B2PLYP-D3), as well as the mPW2PLYP.[35] We have also finally employed the Møller−Plesset perturbation theory,[37] including up to second-order corrections (MP2).

The aug-cc-PVTZ basis set[38] was used for orbital expansion to solve the Kohn−Sham or HF equation iteratively. The "ultrafine" pruned (99,590) grid (99 radial and 590 angular integration points) was used in numerical integration in all DFT calculations. In parallel, just for comparison purposes, we also performed the same calculations with the density functional tight binding method (DFTB). In particular, we have used the DFTB variant with analytical computation of the relevant matrix elements (DFTB-A[39]).

The interaction energies for the located minima on all studied potential energy surfaces of the title system were evaluated, accounting explicitly for the relevance of deformation energy terms, following the approach elaborated by Xantheas.[40] Following the original notation from ref 40, $E_G^{\sigma}(M)$ denotes the electronic energy of the molecule M within the geometry G, calculated with the basis set σ. The interaction energy of a dimer AB is given by

$$\Delta E = E_{AB}^{\alpha\cup\beta}(AB) - E_{A}^{\alpha}(A) - E_{B}^{\beta}(B) \quad (1)$$

Much more frequently, however, the interaction energy is expressed as a "vertical" value, i.e., the electronic energy value is computed for the monomers deformed to the within-dimer geometries:

$$\Delta E' = E_{AB}^{\alpha\cup\beta}(AB) - E_{AB}^{\alpha}(A) - E_{AB}^{\beta}(B) \quad (2)$$

The full counterpoise-corrected interaction energy of the dimer is

$$\Delta E(\mathrm{fCP}) = E_{AB}^{\alpha\cup\beta}(AB) - E_{AB}^{\alpha\cup\beta}(A) - E_{AB}^{\alpha\cup\beta}(B) \quad (3)$$

The basis set superposition error can thus be expressed as

$$\mathrm{BSSE} = \Delta E(\mathrm{fCP}) - \Delta E' \quad (4)$$

Accounting for the monomer deformation energies and avoiding the inconvenience that eqs 1 and 3 do not converge to the same value at the complete basis set limit, the best way to express the counterpoise-corrected interaction energy is

$$\Delta E(\mathrm{BSSE}) = E_{AB}^{\alpha\cup\beta}(AB) - E_{AB}^{\alpha\cup\beta}(A) - E_{AB}^{\alpha\cup\beta}(B) + E_{rel}^{\alpha}(A) + E_{rel}^{\beta}(B) \quad (5)$$

where the E_{rel}-s denote the monomer relaxation energies, given by

$$E_{rel}^{\alpha}(A) = E_{AB}^{\alpha}(A) - E_{A}^{\alpha}(A) \quad (6)$$

$$E_{rel}^{\beta}(B) = E_{AB}^{\beta}(B) - E_{A}^{\beta}(A) \quad (7)$$

This allows us to recast eq 5 as

$$\Delta E(\mathrm{BSSE}) = \Delta E - [E_{AB}^{\alpha\cup\beta}(A) - E_{AB}^{\alpha}(A)] - [E_{AB}^{\alpha\cup\beta}(B) - E_{AB}^{\beta}(B)] \quad (8)$$

The terms in brackets (eq 8) tend to zero upon increase of the basis sets α and β toward the complete basis set (CBS) limit, and therefore ΔE(BSSE) converges to the same result with ΔE in the CBS limit.

2.2. Theoretical Approach to Computation of Anharmonic Vibrational Frequencies. To compute the anharmonic vibrational frequencies for the O−H stretching modes of the free protonated betaine molecule (betaineH(+)) as well as of betaineH(+) interacting with molecular hydrogen, we have adopted the following approach.

First, we carried out a thorough exploration of the potential energy hypersurfaces (PESs) of the investigated systems using all of the previously mentioned levels of theory. The character of the stationary points on the PESs (located by Schlegel's algorithm) was further tested by performing analytical calculations of the Hessian matrices. The absence of negative eigenvalues of the Hessians indicated that a true minimum of the PES is in question. At the same time, by diagonalization of the mass-weighted Hessians, we have calculated the harmonic vibrational frequencies.

Subsequently, to compute the anharmonic vibrational potential of the O−H stretching mode, which is essentially localized and decoupled from all other intra- and intermolecular modes, we have generated a series of configurations in which the positions of all atoms and the center of mass of the O−H oscillator were kept fixed, while only the O and H atoms were moved in opposite directions, according to the following equations of motion:

https://doi.org/10.1021/acs.jpca.4c01331
J. Phys. Chem. A 2024, 128, 3968−3981

$$\vec{r}(\mathrm{O}) = \frac{m_{\mathrm{H}}}{m}\cdot\vec{r} \tag{9}$$

$$\vec{r}(\mathrm{H}) = \frac{m_{\mathrm{O}}}{m}\cdot\vec{r} \tag{10}$$

where

$$\vec{r} = \vec{r}(\mathrm{H}) - \vec{r}(\mathrm{O}) \tag{11}$$

Further, we have carried out a series of single-point energy calculations for each of the generated configurations in the case of all considered O−H oscillators. A total of 20 single-point calculations were carried out for each of the O−H oscillators considered, varying the O−H distance from 0.70 to 1.65 Å. The obtained vibrational potential energy curves:

$$V = f(r_{\mathrm{OH}}) \tag{12}$$

were subsequently used to solve the vibrational Schrödinger equation numerically by implementating of Numerov's method.

To evaluate the influence of geometry distortion of the betaineH(+) subunit induced by interaction with molecular hydrogen on the O−H stretching frequencies and frequency shifts, we have also computed the O−H stretching potentials and subsequently solved the vibrational Schrödinger equation for distorted betaineH(+) molecules within the dimer geometry (excluding the hydrogen subunit).

2.3. Charge Field Perturbation Analysis of the Vibrational Potential. To gain further insight into the forces governing the observed O−H frequency red shift and the corresponding implications for the type of this noncovalent interaction, a charge field perturbation (CFP) analysis of the O−H stretching vibrational potential has been carried out.[20] The CFP procedure consisted of the following steps. First, the charge distribution in the H_2 molecule under the influence of the protonated betaineH(+) unit in the geometry arrangement corresponding to the minima on the HCTH/aug-cc-pVTZ PES was calculated by fitting the atom-centered point charges to the electrostatic potential obtained from the HCTH/aug-cc-pVTZ KS electron density at a series of points chosen with the CHELPG selection algorithm. Subsequently, the O−H stretching vibrational potential of the protonated betaineH(+) in the field generated by the system of these two point charges was calculated in a completely analogous manner as in the full-wave function representation of both monomeric units within the dimer. The resulting vibrational Schrödinger equation has been solved for this case with the Numerov's method as well.

2.4. NBO Deletion Analysis of the Vibrational Potential. In order to get additional, in some aspects, even more in-depth physical insights into the factors governing the O−H stretching frequency shifts of the betaineH(+) cation interacting with the neutral hydrogen molecule as a "tagger," we have carried out a natural bond orbital (NBO) deletion analysis for each point of the vibrational potential $V(r_{\mathrm{OH}})$. For each point of the series, we first solved the KS equations at the HCTH/aug-cc-pVTZ level of theory. In the converged KS analogue of the Fock matrix, subsequently, all of the matrix elements corresponding to the intermolecular charge transfer (CT), of the form:

$$\langle \psi^{\mathrm{donor}}_{\mathrm{betaine}(+)} | \hat{F} | \psi^{\mathrm{acceptor}}_{\mathrm{H2}} \rangle \tag{13}$$

as well as

$$\langle \psi^{\mathrm{donor}}_{\mathrm{H2}} | \hat{F} | \psi^{\mathrm{acceptor}}_{\mathrm{betaine}(+)} \rangle \tag{14}$$

were set to zero, and the newly obtained Fock matrix was diagonalized to obtain the new density matrix, which was subsequently passed through only a single SCF step. In this way, we eliminated all of the intermolecular delocalizations of the electronic density, which would occur from the high-occupancy orbitals of one to the low-occupancy orbitals of the other monomeric unit within the dimer. We can therefore study the O−H stretching vibrations without any CT between betaineH(+) and hydrogen in both directions.

2.5. Second-Generation Absolutely Localized Molecular Orbitals Energy Decomposition Analysis (ALMO-EDA 2) of the Vibrational Potential. To get further insights into the physics governing the observed O−H stretching frequency shifts in the studied weakly interacting dimers, we have carried out the second-generation absolutely localized molecular orbital energy decomposition analysis (ALMO-EDA 2) at each point of the O−H stretching vibrational potential. Within the ALMO-EDA 2 decomposition scheme, the intermolecular interaction energy ΔE_{int} (defined as a difference between the full energy of the complex E_{full} and the sum of fragment energies $\Sigma\Delta E_{\mathrm{f},i}$) is represented as a sum of dispersion (ΔE_{disp}), Pauli repulsion ($\Delta E_{\mathrm{Pauli}}$), permanent electrostatics (ΔE_{elec}), polarization (ΔE_{pol}), and charge-transfer (ΔE_{ct}) contributions:

$$\begin{aligned}\Delta E_{\mathrm{int}} &= E_{\mathrm{full}} - \sum_i \Delta E_{\mathrm{f},i} \\ &= \Delta E_{\mathrm{disp}} + \Delta E_{\mathrm{Pauli}} + \Delta E_{\mathrm{elec}} + \Delta E_{\mathrm{pol}} + \Delta E_{\mathrm{ct}}\end{aligned} \tag{15}$$

This approach is variational and is based on valid antisymmetrized electronic wave functions in producing the interaction energy contributions in eq 15. The scheme works with single-determinant Kohn−Sham densities as well. Aside from its descriptivism, the terms that it generates have clear physical meaning, a correct sign, and asymptotic behavior, as well as a physically valid complete basis set limit. The exact expressions through which each of the terms in eq 15 has been computed are given in refs 21,22.

3. RESULTS AND DISCUSSION

Two minima that have been located on all of the studied PESs of the betaineH(+)−H_2 dimer are shown in Figure 1. Minimum 1 (a) is a T-shaped structure in which the carboxylic O−H group points directly toward the center of the H−H bond. It corresponds to the tagging of the O−H group. Such a T-shaped arrangement, considering the multipole moments of the two interacting molecules, could, in principle, imply a favorable dipole−quadrupole interaction (aside from the charge−quadrupole term). Minimum 1 (b), on the other hand, corresponds to the tagging of the charged group of protonated betaineH(+).

Figure 2 shows the direction of the dipole moment vector of the noncovalently bonded dimer of the protonated betaineH-(+) and molecular hydrogen as a tagger. It effectively coincides with the dipole moment vector of the free betaineH(+). The dipole−quadrupole interaction energy component for a dipole μ_{A} and a linear quadrupole Θ_{B} directed along the z-axis of a local coordinate system can be computed with[41]

https://doi.org/10.1021/acs.jpca.4c01331
J. Phys. Chem. A 2024, 128, 3968−3981

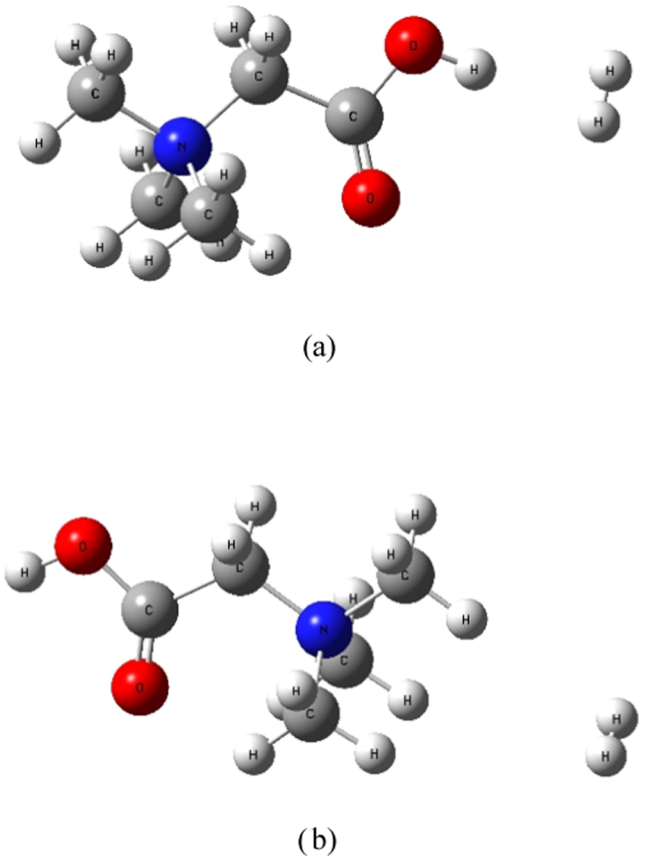

Figure 1. Minima located on the studied PESs of the betaineH(+)–H_2 noncovalently bonded dimer.

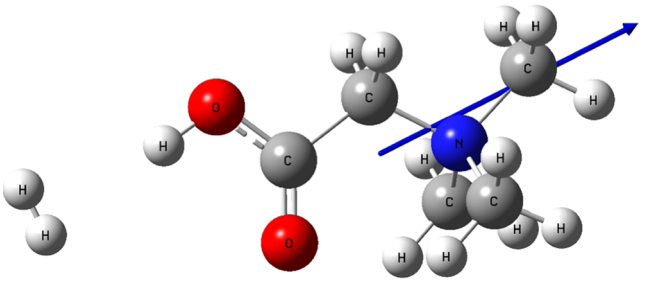

Figure 2. Direction of the dipole moment vector of the noncovalently bonded dimer of the protonated betaineH(+) and molecular hydrogen as a tagger, which effectively coincides with the dipole moment vector of the free betaineH(+).

$$U_{\mu\Theta} = \frac{\mu^{A}\Theta^{B}}{4\pi\varepsilon_0 R^4}\cdot\frac{3}{2}[\cos\theta_A(3\cos^2\theta_B - 1) - \sin\theta_A \sin 2\theta_B \cos\varphi] \quad (16)$$

with $\varphi = \varphi_B - \varphi_A$. In the case of an orientation such as in the T-shaped minimum on the PES, schematically shown in Figure 3 ($\theta_A = \pi$, $\theta_A = \pi/2$), $U_{\mu\Theta}$ reduces to

$$U_{\mu\Theta} = \frac{\mu^{A}\Theta^{B}}{4\pi\varepsilon_0 R^4}\cdot\frac{3}{2} \quad (17)$$

In other words, the dipole–quadrupole term alone will destabilize the noncovalent interaction in the present case. Therefore, charge transfer must play a significant role in stabilizing the dimer geometry.

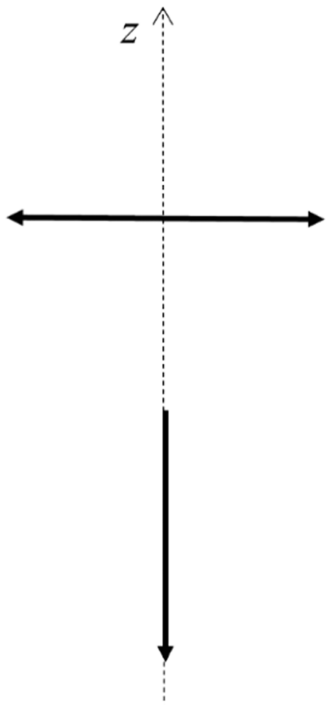

Figure 3. Mutual orientation of the dipole and quadrupole moments of the interacting molecules in the T-shaped minimum corresponding to H_2 tagging of the OH group of the protonated betaineH(+); see text for details.

Tables SI-I and SI-II summarize the interaction energies for the two minima located on the dimer's PES at all of the considered theoretical levels. In the case of betaineH(+) tagged from the OH side, the ΔE(fCP) values span the range from 1.3 to approximately 2.0 kcal/mol (Table SI-I). Long-range-corrected functionals tend to increase the interaction energies, and the same conclusion holds for the dispersion-corrected ones, too. Concerning the deformation energy contributions, as can be seen from the ΔE(BSSE) values, these seem to contribute most at B3LYP, CAM-B3LYP, and HCTH/407 levels of theory. As for the minimum corresponding to the betaineH(+) tagged from the methylated, i.e., charged side (Table SI-II), the ΔE(fCP) and $\Delta E'$ values tend to be systematically lower than the corresponding ones for the OH-tagged analogue. Upon inclusion of the deformation energies, however, the interaction energy decrease tends to be the smallest at the previously mentioned B3LYP, CAM-B3LYP, and HCTH/407 levels of theory.

Tables SI-III–SI-V (see the Supporting Information) summarize the results from the harmonic as well as the anharmonic vibrational analyses, i.e., the frequencies (wavenumbers) of the fundamental $|0\rangle \rightarrow |1\rangle$ vibrational transitions corresponding to the O–H stretching modes in the case of free betaineH(+) and betaineH(+)···H_2, with the H_2 tagging realized on the CH_3 and OH sides, and the corresponding frequency shifts calculated according to the described procedure together with the available experimental IRMPD data.[7]

As can be seen from the calculated O–H stretching frequency shifts from the harmonic vibrational analysis, all levels of theory are in good agreement with experimental data corresponding to the OH-tagged minimum, with a notable overestimation of the absolute values of the frequency shifts.

https://doi.org/10.1021/acs.jpca.4c01331
J. Phys. Chem. A 2024, 128, 3968–3981

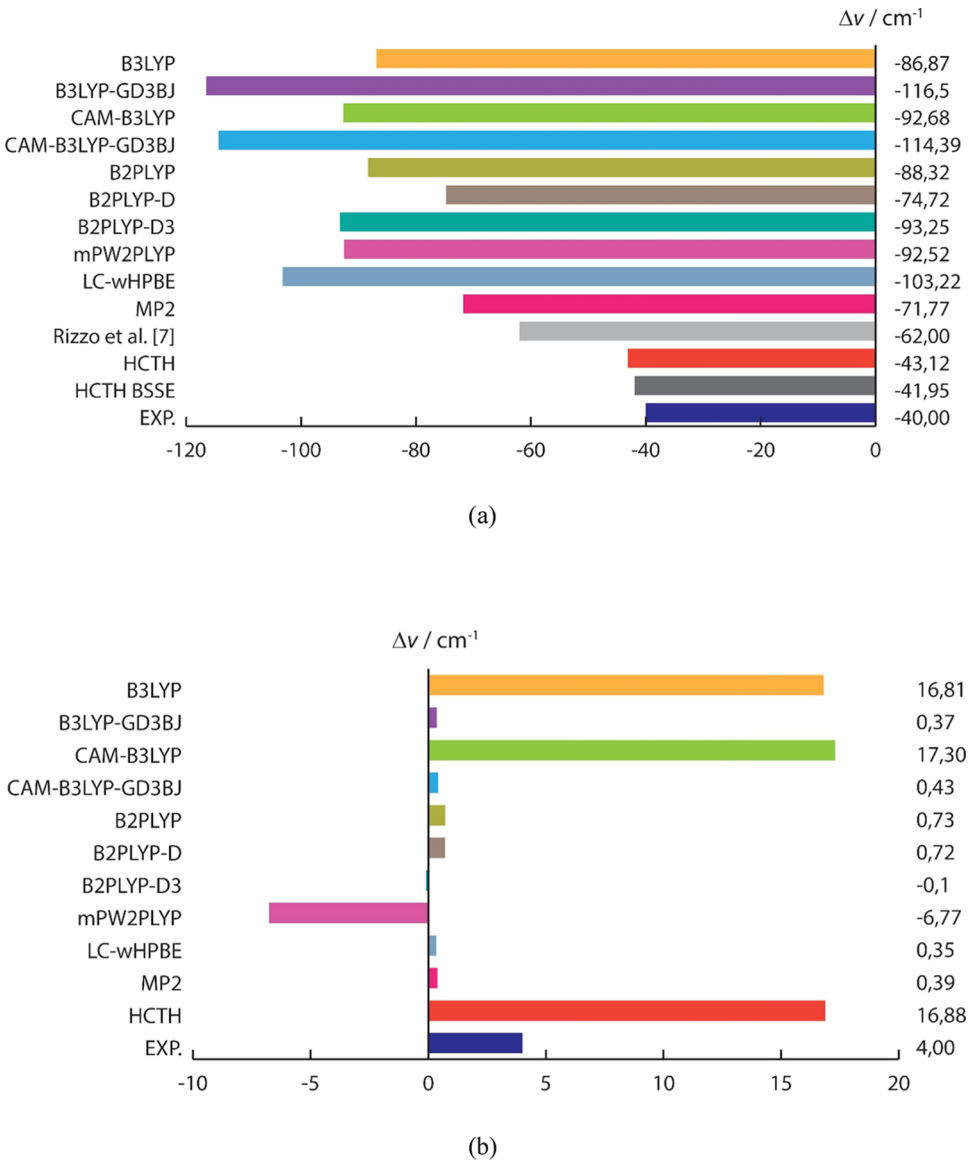

Figure 4. Anharmonic frequency shifts of the fundamental $|0\rangle \rightarrow |1\rangle$ vibrational transitions corresponding to the O−H stretching modes calculated at different levels of theory in the case of (a) OH-tagged and (b) charge side-tagged dimer.

The only exception is the HCTH level of theory, at which the frequency shift is underestimated. At the same time, values calculated with the long-range-corrected functionals tend to give only slightly higher (in absolute value) frequency shifts, while inclusion of the dispersion correction leads to a significant increase of the absolute values of the frequency shifts and a significantly worse agreement with the experiment. The second-order Møller−Plesset perturbation theory results outperform all DFT methods. Concerning the minimum corresponding to the charged side tagging, all levels of theory except B3LYP, CAM-B3LYP, and HCTH predict a very small frequency blue shift, less than 1 cm^{-1}. Considering the counterpoise-corrected PESs does not change the results significantly, regardless of the level of theory.

Harmonic frequencies and frequency shifts, however, can be viewed only as a first approximation to a realistic description of the vibrational dynamics of X-H oscillators containing a light atom that can exhibit large amplitude motions. We therefore consider our results obtained by the previously elaborated anharmonic computational procedure as far more relevant in the course of comparison to the experimental data. It has been recognized, at the same time, that unlike the harmonic frequencies and the corresponding frequency shifts calculated with the DFT methodology, which can sometimes be in fortuitous agreement with the experimental data, the anharmonic counterparts often significantly overestimate the observed values.[8,9,15] However, this aspect has not received the attention that it certainly deserves. The mentioned overestimation of the anharmonic frequency shifts has often been attributed to overestimation of the hydrogen bond strengths at DFT levels of theory. It has also been implied that neglect of the dispersion interactions and the inappropriate long-range behavior of many of the widely used DFT functionals could cause such an overestimation. To the best of our knowledge, this is the first study that addresses all of these aspects in a systematic way. Finding an optimal DFT functional which would provide a good match to the experimental data would be of both practical and fundamental significance, as such functional should have a rather balanced behavior in all of these aspects and therefore pave the way toward construction

https://doi.org/10.1021/acs.jpca.4c01331
J. Phys. Chem. A 2024, 128, 3968−3981

of even better functionals suitable for modeling noncovalent intermolecular interactions.

In the case of minimum corresponding to the protonated betaine cation tagged from the OH side (Table SI-IV, see the Supporting Information), the anharmonic O−H stretching frequency shifts overestimate much more significantly the experimental data as compared to the harmonic ones, with only a single notable exception: the HCTH/407 functional. The effect becomes even much more pronounced upon using long-range-corrected variants of the functionals and especially upon inclusion of the dispersion corrections. A firm rationalization of such observations can be offered by the following arguments. Upon O−H bond stretch, the vibrating hydrogen atom, spanning more and more through the anharmonic region of the cut through the vibrational PES, comes in closer proximity to the hydrogen molecule. The enhanced dispersion energy contributions to dimer stabilization at such smaller distances subsequently lower the potential energy curve in this region and inevitably cause a very high O−H stretching frequency red shift. As for the anharmonic O−H stretching frequency shifts in the case of minimum II (betaineH(+) tagged from the charged side), the same conclusions are valid as in the discussion of harmonic frequency shifts: small blue shifts often close to 1 cm^{-1}, with four notable exceptions: the B3LYP, CAM-B3LYP, HCTH, and mPW2PLYP levels of theory. The calculated anaharmonic O−H stretching frequency shift values summarized in Table SI-V (see the Supporting Information) reflect the contribution of the geometry distortion of the betaineH(+) subunit upon interaction with molecular hydrogen on the O−H stretching vibrational potential. As can be seen, the deformation-induced shifts are all in the "blue" direction (i.e., upshifts) when one considers betaineH(+) tagged from the side of the OH group and are sometimes quite notable (e.g., ∼17.7 cm^{-1} at the HCTH/407 level). The most viable rationalization of such findings (outlined in detail in Tables SI-IV and V as well as in Figure 4) lies in the following argumentation. The interaction-induced geometry distortion, i.e., its overestimation at certain levels of theory in the case of charge side-tagged minimum II (which appears to depend strongly on the dispersion correction), leads to overestimated deformation of the O−H stretching vibrational potential even in the case when there is no direct O−H···H_2 contact. Hence, the frequency shift of the O−H stretching vibration is overestimated as well. Aside from the inappropriate description of the dispersion energy terms, overestimation of the charge-transfer terms could contribute to the overall effect, too.

The overall performance of all theoretical approaches implemented in the present study is pictorially illustrated in Figures 4 and SI-1 (see the Supporting Information).

Since the HCTH/407 functional designed by Handy and coworkers has significantly outperformed all of the other levels of theory employed in the present study (including MP2 and the double-hybrid methodologies as well), all additional analyses and insights have been gained with this functional.

To gain additional insight into the factors governing the O−H stretching frequency shift induced by the interaction of betaineH(+) with molecular hydrogen, we have considered the CFP and NBO deletion approaches, as explained in Section 2. Figures 5 and 6 depict the computed O−H stretching vibrational potentials by the full-wave function method, as well as by the CFP and NBO deletion methods for both minima located on the HCTH/407/aug-cc-pVTZ PES. Table 1, on the other hand, summarizes the vibrational frequencies and the corresponding frequency shifts.

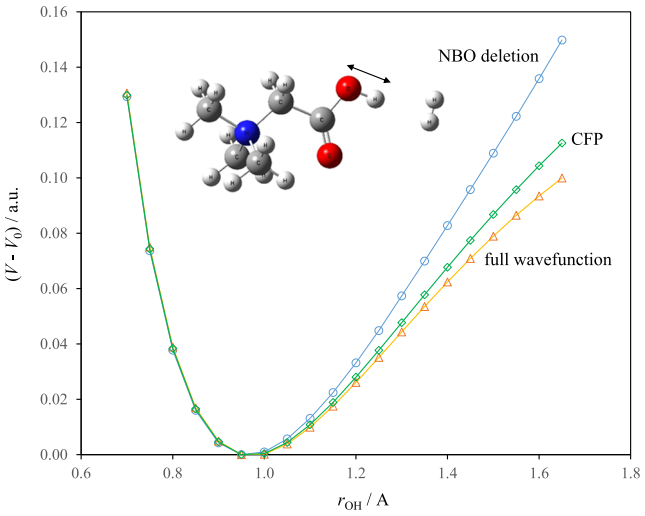

Figure 5. O−H stretching vibrational potentials of the OH-tagged structure computed by the full-wave function method, as well as by the CFP and NBO deletion methods at the HCTH/407/aug-cc-pVTZ level of theory.

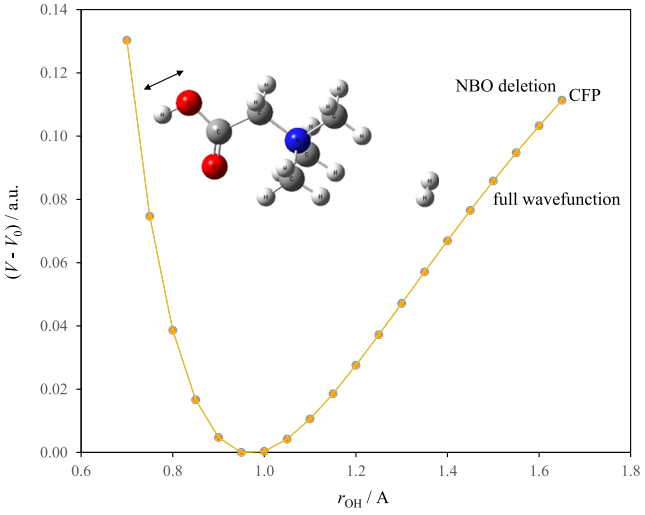

Figure 6. O−H stretching vibrational potentials of the charged side-tagged structure computed by the full-wave function method, as well as by the CFP and NBO deletion methods at the HCTH/407/aug-cc-pVTZ level of theory.

As can be seen, in the case of minimum corresponding to betaineH(+) tagged by molecular hydrogen from the charged side, the full-wave function values coincide with both the CFP and NBO deletion ones. We can therefore safely conclude that the charge-transfer interaction does not influence the O−H stretching frequency shifts in the case of this minimum, and the overall effect can be attributed to the electrostatic field generated by the hydrogen as a molecular tagger. The situation is, however, drastically different when one considers the minimum corresponding to betaineH(+) tagged from the OH group side.

Evidently, the electrostatic interaction-induced frequency shift will be a significant blue shift, which is quite contrary to what is experimentally observed. At the same time, elimination of the intermolecular charge transfer would cause a drastic

https://doi.org/10.1021/acs.jpca.4c01331
J. Phys. Chem. A 2024, 128, 3968−3981

Table 1. Calculated Anharmonic Frequencies and Frequency Shifts of the Fundamental $|0\rangle \rightarrow |1\rangle$ Vibrational Transitions Corresponding to the O−H Stretching Modes in the Case of Betaine(+)···H_2, with the H_2 Tagging Realized on the OH and Charged Sides with the Full-Wave Function Approach, Charge Field Perturbation Approach, and the NBO Deletion Method

HCTH		ν (cm^{-})	$\Delta\nu$ (cm^{-1})
minimum 1	full wfn.	3465.99	−43.12
	CFP	3539.96	30.84
	NBO−DEL	3731.77	222.66
minimum 2	full wfn.	3525.99	16.88
	CFP	3525.26	16.15
	NBO−DEL	3525.69	16.58

frequency blue shift again. We have therefore concluded that the experimentally observed red shift in the frequency of the O−H stretching vibrational can be attributed to the intermolecular charge transfer from the hydrogen molecule to the O−H group of betaineH(+). Frequency-wise, therefore, the betaineH(+)···H_2 dimer behaves as a typical hydrogen-bonded system.

To further investigate the nature and strength of non-covalent bonding in the betaineH(+)···H_2 dimer, we have carried out Bader's (i.e., atoms in molecules—AIM) analysis of the topology of the electronic density,[16] as well as the noncovalent interactions (NCI) analysis.[19]

We have searched for critical points of the electronic density scalar fields of both dimers (corresponding to realization of tagging from both OH and charged sides), identified their types, and subsequently calculated the charge densities $\rho(\vec{r}_c)$ and the corresponding density Laplacians $\nabla^2\rho(\vec{r}_c)$ at these positions. All calculations in this context were performed for the electronic density scalar field calculated for minimums I and II at the HCTH/407/aug-cc-pVTZ level of theory. The critical points are characterized by the condition:

$$\nabla\rho(\vec{r}_c) = 0 \tag{18}$$

Their character has further been explored by calculating the eigenvalues of the corresponding Hessian computed at $\vec{r}_c$:

$$\Lambda = \begin{pmatrix} \frac{\partial^2\rho}{\partial x^2} & 0 & 0 \\ 0 & \frac{\partial^2\rho}{\partial y^2} & 0 \\ 0 & 0 & \frac{\partial^2\rho}{\partial z^2} \end{pmatrix}_{\vec{r}=\vec{r}_c} = \begin{pmatrix} \lambda_1 & 0 & 0 \\ 0 & \lambda_2 & 0 \\ 0 & 0 & \lambda_3 \end{pmatrix} \tag{19}$$

We have located several critical points with rank 3 and signature −1, briefly denoted as (3, −1) critical points or bond critical points—BCPs. The molecular graph, together with the (3, −1) BCPs and bond paths in the case of betaineH(+)···H_2 dimer with tagging on the OH group side, is presented in Figure 7.

The (3, −1) BCP located on the bond path between the OH group H20 atom and the center of the H−H σ bond is the most important in this context. The calculated $\rho(\vec{r}_c)$ value at this critical point is 0.008 au, while the $\nabla^2\rho(\vec{r}_c)$ value, defined as the trace of matrix (18), is 0.02557 au. Both the $\rho(\vec{r}_c)$ and the $\nabla^2\rho(\vec{r}_c)$ values at this critical point fall within the range defined as a basic criterion for the existence of hydrogen bond by Popelier,[42] though the electron density Laplacian tends to be close to the lower limit. The (3, −1) BCPs between methyl group protons H10 and H17 and O18 atom are, on the other hand, symmetry-equivalent, both being characterized with $\rho(\vec{r}_c)$ = 0.012 au, and $\nabla^2\rho(\vec{r}_c)$ = 0.04877 au.

The NCI analysis is based on the construction of the plot of the so-called reduced density gradient (RDG) vs the electronic density ρ, or sign$(\lambda_2)\cdot\rho$, calculated from the HCTH/407/aug-cc-pVTZ KS wave function. The reduced density gradient is defined as

$$s = \frac{1}{2(3\pi^2)^{1/3}}\frac{|\nabla\rho|}{\rho^{4/3}} \tag{20}$$

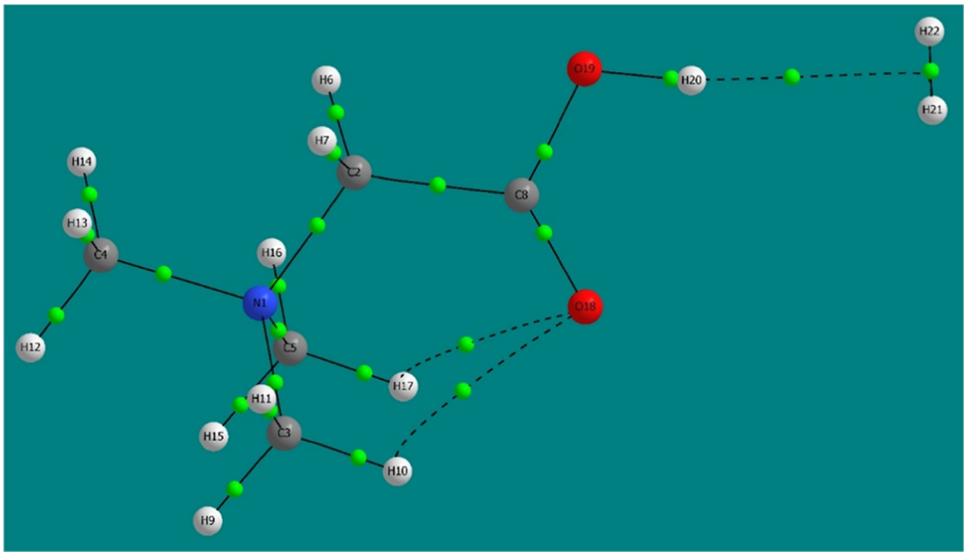

Figure 7. Molecular graph, together with the (3, −1) BCPs and bond paths in the case of betaineH(+)···H_2 dimer with tagging on the OH group computed by Bader analysis at the HCTH/407/aug-cc-pVTZ level of theory.

https://doi.org/10.1021/acs.jpca.4c01331
J. Phys. Chem. A 2024, 128, 3968−3981

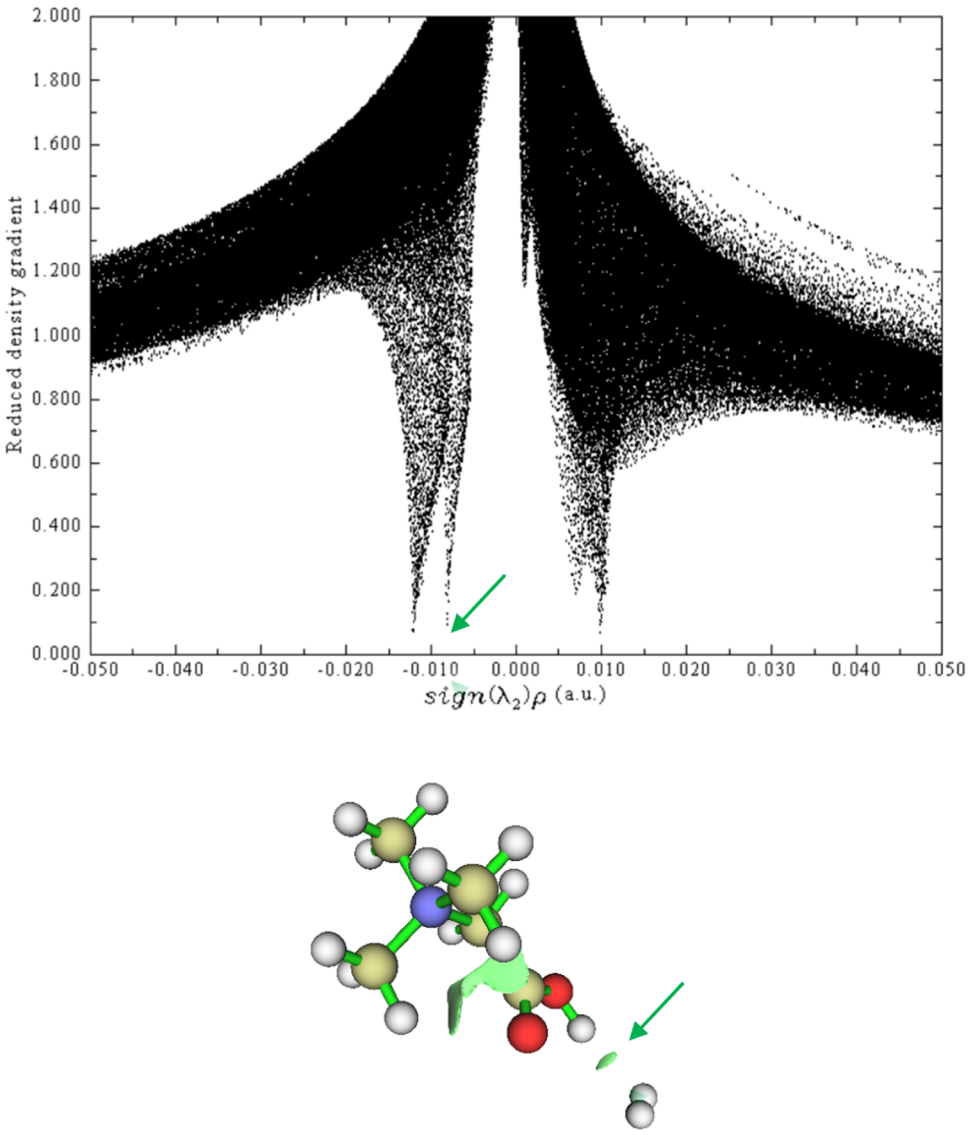

Figure 8. Scatterplot of s vs sign$(\lambda_2)\cdot\rho$ for the OH-tagged minimum located on the betaineH(+)···H_2 dimer HCTH/407/aug-cc-pVTZ PES, together with the NCI isosurface.

This quantity is an excellent indicator of weak intra- or intermolecular noncovalent interactions. In the region of low electronic density and high gradient, which corresponds to NCIs, crucial changes appear in the RDG and a consequent appearance of through associated with each of the critical points of the electronic density gradient field. As it is the electron density Laplacian sign that determines the character of the net gradient flux, it directly indicates the electronic density concentration or depletion at the critical point relative to its surroundings. The second eigenvalue λ_2 of the Hessian computed at $\vec{r}_c$ ($\lambda_1 < \lambda_2 < \lambda_3$) determines the electronic density variation in the plane normal to the eigenvector λ_3 while its sign directly determines the accumulation or depletion of energy density and hence the interaction type.

Figures 8−10 show the scatterplots of s vs sign$(\lambda_2)\cdot\rho$ for the two minima located on the betaineH(+)···H_2 dimer HCTH/407/aug-cc-pVTZ PES, as well as for the betaineH(+) monomer, together with the NCI isosurfaces.

As can be seen from Figure 8, the sign$(\lambda_2)\cdot\rho$ value for the OH···H_2 contact is negative, indicating the attractive character of this interaction. It is, however, weaker than the intramolecular attractive CH···O interactions, which are characterized by a more negative sign$(\lambda_2)\cdot\rho$ value. The minimum where tagging is realized from the charged side, as can be seen from Figure 9, is characterized by two contacts: one with a negative sign$(\lambda_2)\cdot\rho$ value and the other with a positive one. Both are, however, characterized by very small absolute values.

In addition, we have also analyzed the charge-transfer interaction in the studied dimer, using second-order perturbation theory (SOPT) estimates of the donor−acceptor orbital interactions on the natural bond orbital (NBO) basis.[17,18,43] In this approach, the SOPT estimate of the energetic effects of the charge-transfer interaction between orbitals i and j is given by

$$E^{(2)} = \Delta E_{ij} = q_i \cdot \frac{|\langle \psi_i | \hat{F} | \psi_j \rangle|^2}{\varepsilon_i - \varepsilon_j} \tag{21}$$

In eq 20, q_i is the occupancy of the donor orbital, and $\langle \psi_i | \hat{F} | \psi_j \rangle$ is the nondiagonal matrix element of the Fock operator in the NBO basis, while ε_i and ε_j are the orbital energies. Table 2 summarizes the results from the SOPT analysis for both

https://doi.org/10.1021/acs.jpca.4c01331
J. Phys. Chem. A 2024, 128, 3968−3981

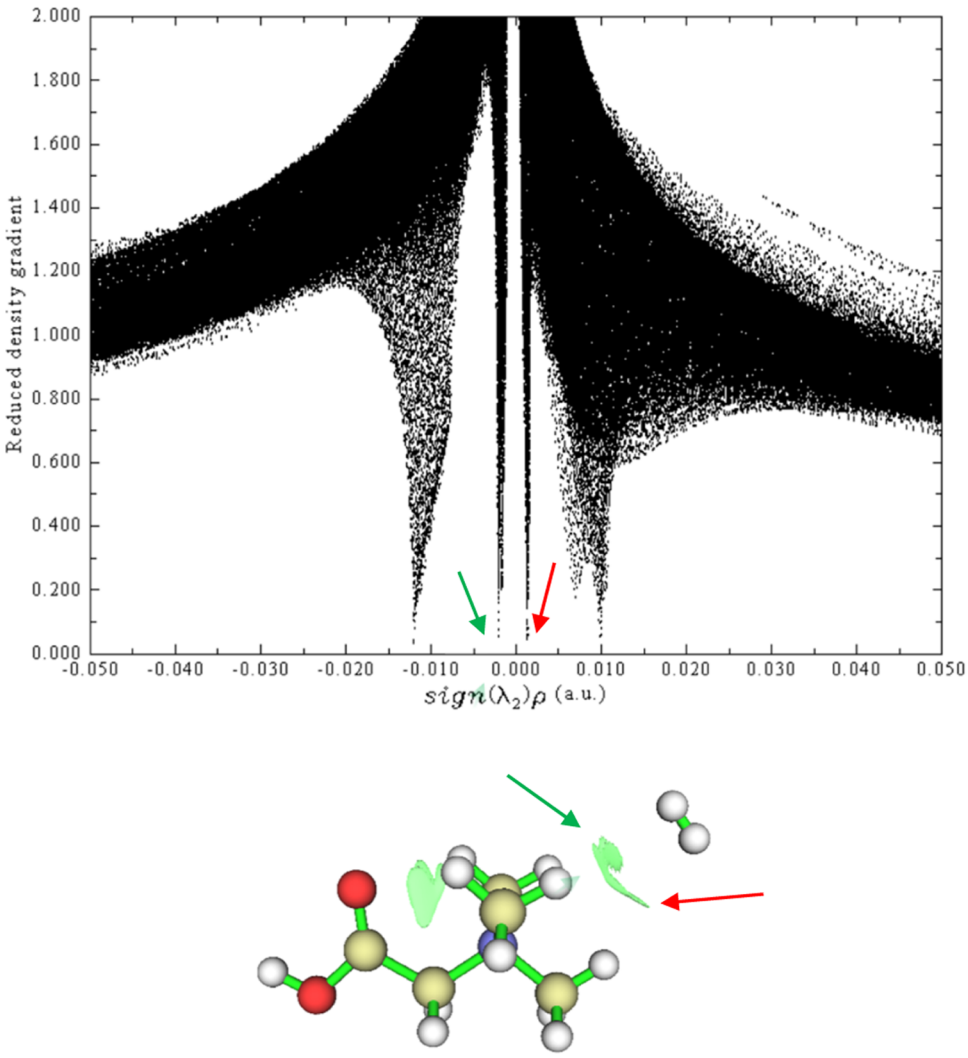

Figure 9. Scatterplot of s vs sign(λ_2)·ρ for the charged side-tagged minimum located on the betaineH(+)···H_2 dimer HCTH/407/aug-cc-pVTZ PES, together with the NCI isosurface.

minima on the HCTH/407/aug-cc-pVTZ PES of the betaineH(+)···H_2 dimer.

As can be seen, charge-transfer interaction occurs in both minima, with the σ_{HH} orbital playing the role of an electron donor. In the case of dimer representing betaineH(+) tagged from the OH group side, the antibonding O−H orbital plays the role of electron acceptor, and the overall energetic effect of this charge delocalization interaction is quite significant. The quantity of the transferred charge, although being small on an absolute scale, is significant in the sense of noncovalent intermolecular interactions. One-directional CT from the tagger H_2 molecule to the protonated betaineH(+) molecule also exists in the minimum representing the tagging situation from the charged side. It involves the two σ^*(C−H) orbitals in which the hydrogen atoms H9 and H15 from the CH_3 groups of the betaineH(+) moiety take part. These are exactly the same atoms for which a stabilizing noncovalent contact has been established by the NCI RDG analysis. This interaction is, however, much less significant than the one in the case of the first minimum. The NBO results are thus quite consistent with the conclusions derived on the basis of the NCI RDG analyses.

Finally, the dependencies of the interaction energy terms calculated by the second-generation ALMO-EDA 2 approach (defined in expression 15) on the O−H distance upon excitation of the O−H stretching mode in the case of two minima located on the HCTH/407/aug-cc-pVTZ PES are shown in Figures 11 and 12. As can be seen, in the case of OH-tagged minimum, which is of primary importance for the present study, the permanent electrostatics (ΔE_{elec}), polarization (ΔE_{pol}), and charge-transfer (ΔE_{ct}) contributions to the total intermolecular interaction energy ΔE_{int} contribute favorably to the weak hydrogen bond formation and the red shift of the fundamental O−H stretching frequency. In the case of all of these contributions:

$$\frac{d(\Delta E_i)}{dr_{OH}} < 0 \tag{22}$$

The Pauli repulsion term, on the other hand, clearly favors the O−H stretching frequency blue shift:

$$\frac{d(\Delta E_{Pauli})}{dr_{OH}} > 0 \tag{23}$$

The dispersion energy component does not seem to contribute significantly to the O−H stretching frequency shift, as in this case:

https://doi.org/10.1021/acs.jpca.4c01331
J. Phys. Chem. A 2024, 128, 3968−3981

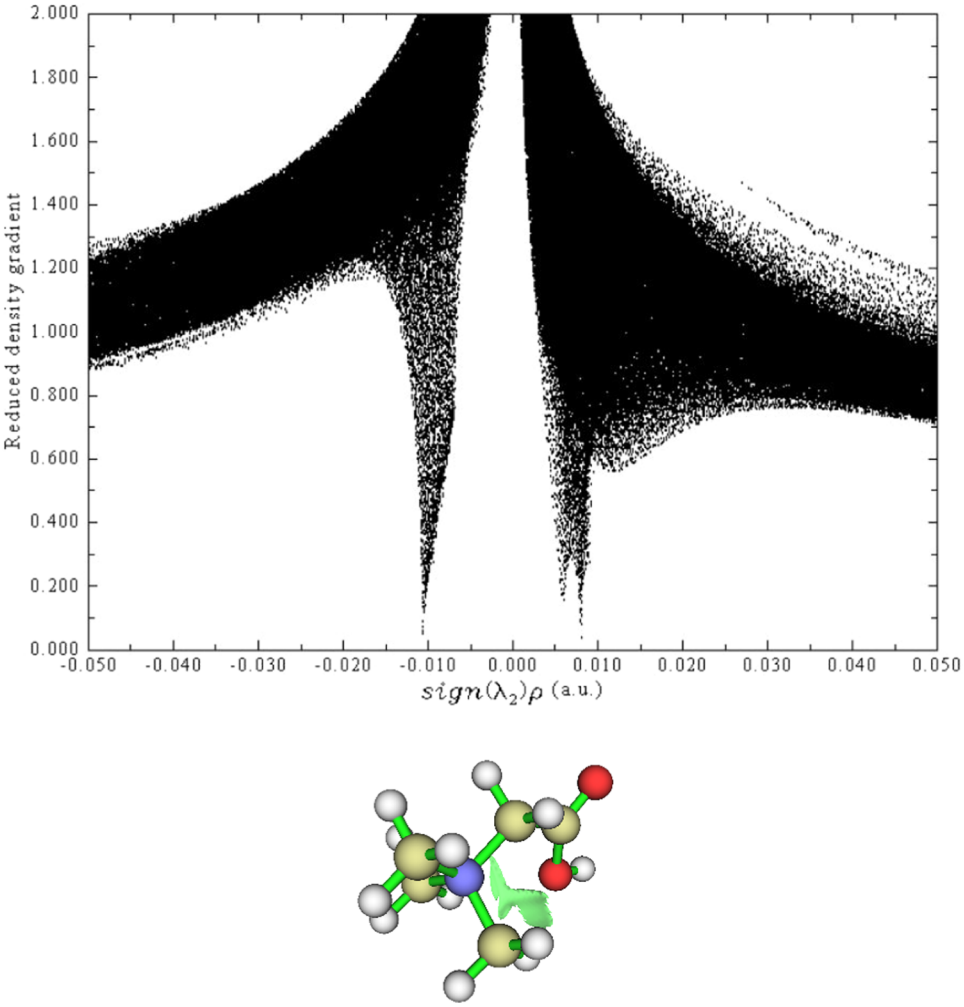

Figure 10. Scatterplot of s vs sign$(\lambda_2)\cdot\rho$ for the minimum located on the free betaineH(+) HCTH/407/aug-cc-pVTZ PES, together with the NCI isosurface.

Table 2. Results from the Second-Order Perturbation Theory (SOPT) Estimates of the Donor−Acceptor Orbital Interactions in the Natural Bond Orbital (NBO) Basis for Both Minima on the HCTH/407/aug-cc-pVTZ PES of the BetaineH(+)···H_2 Dimer

	ψ_{donor}	$\psi_{acceptor}$	$E^{(2)}$ (kcal/mol)	$(\varepsilon_i - \varepsilon_j)$ (au)	$\langle\psi_i\lvert\hat{F}\rvert\psi_j\rangle$ (au)
		OH-Tagged Minimum			
	σ(H−H)	σ^*(O−H)	1.16	0.69	0.025
		Charge-side-tagged Minimum			
C−H9	σ(H−H)	σ^*(C−H)	0.07	0.67	0.006
C−H15	σ(H−H)	σ^*(C−H)	0.07	0.67	0.006

$$\left(\frac{\mathrm{d}(\Delta E_{\mathrm{disp}})}{\mathrm{d}r_{\mathrm{OH}}}\right)_{r_{\mathrm{OH}}\to r_{\mathrm{OH,e}}} \to 0 \tag{24}$$

However, the general trend in the completely investigated r_{OH} region shows that dispersion favors frequency red shift. As can be seen from Figure 11, where the plots of ΔE_{disp}, ΔE_{elec}, ΔE_{pol}, and ΔE_{ct} contributions to the total ΔE_{int} versus r_{OH} are shown, the absolute value of the derivative $(\mathrm{d}(\Delta E_i)/\mathrm{d}r_{OH})_{r_{OH}=r_{OH,e}}$ is highest in the case of the charge-transfer contribution. This derivative for the charge transfer becomes larger in absolute

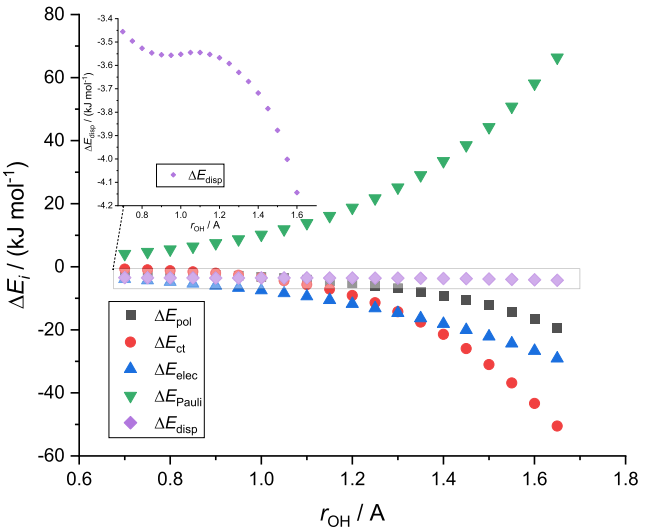

Figure 11. Dependencies of the interaction energy terms calculated by the second-generation ALMO-EDA 2 approach on the O−H distance in the case of OH-tagged minimum located on the betaineH(+)···H_2 dimer HCTH/407/aug-cc-pVTZ PES—the inset represents the r_{OH}-dependence of the dispersion energy term—ΔE_{disp}.

https://doi.org/10.1021/acs.jpca.4c01331
J. Phys. Chem. A 2024, 128, 3968−3981

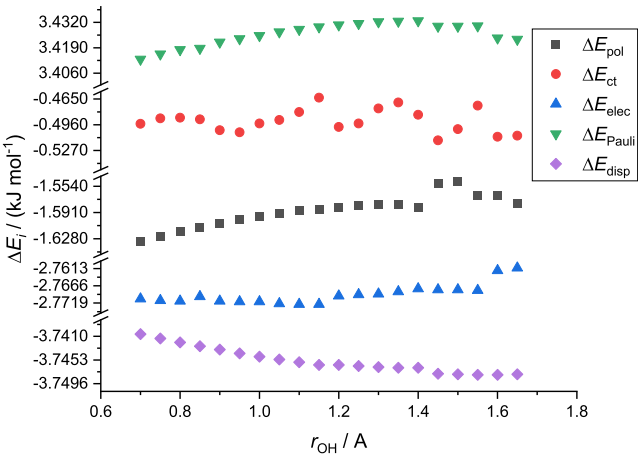

Figure 12. Dependencies of the interaction energy terms calculated by the second-generation ALMO-EDA 2 approach on the O−H distance in the case of charged side-tagged minimum located on the betaineH(+)···H_2 dimer HCTH/407/aug-cc-pVTZ PES.

value at $r_{OH} > r_{OH,e}$, opposite to the case of derivatives of other contributions. From the second-generation ALMO-EDA analysis, we can therefore safely ascribe the largest contribution of the charge-transfer interaction energy term to the overall frequency red shift. These conclusions are fully in line with the NBO analysis.

The blue-shifting contribution of the Pauli repulsion term can, on the other hand, be ascribed to the so-called "vibrational wall-effect," i.e., due to the confinement of the O−H stretching oscillator by the tagging molecule acting as an obstacle to the high-amplitude motion. The anharmonic O−H stretching oscillator, encountering an increase in Pauli repulsion as it approaches the more distant regions of the vibrational PES (thus getting closer to the molecular hydrogen σ-electron density), "sees" an increased vibrational potential energy, i.e., the vibrational potential becomes steeper in comparison to the case when the tagging H_2 molecule is absent.

Analysis of the dependence of different ΔE_i contributions to ΔE_{int} on r_{OH} in the case of the charged side-tagged minimum (Figure 12) leads us to the following conclusions. All contributions, aside from the Pauli repulsion, are negative. In this case, however, the contribution to vibrational blue versus red shifts is much more complex and convoluted. While the Pauli repulsion favors O−H stretching frequency blue shift up to $r_{OH} \approx 1.4$ Å, above this value, the trend changes. Charge transfer, on the other hand, exhibits oscillatory behavior, which may be ascribed to the fluctuations in betaineH(+) charge density upon excitation of the O−H vibration and thus the values of the fragment electric-field response functions (FERFs) that are used in computation of ΔE_{ct} in the ALMO-EDA 2 method.

It is worth mentioning at this point that such oscillations are not observed in the case of OH-tagged minimum, as the general trend of the dependence $\Delta E_{ct}(r_{OH})$ is in that case governed by much larger charge density fluctuations imposed by the arrangement which favors direct σ(H−H) → σ^*(O−H) interaction. The fluctuations thus appear only when the energy contributing term is significantly smaller in absolute value. Both the permanent electrostatics (ΔE_{elec}) as well as the polarization (ΔE_{pol}) terms, in this case, contribute to O−H stretching frequency blue shift (the derivatives $(d(\Delta E_i)/dr_{OH})$ are positive in both cases).

Only the dispersion energy term contributes consistently to the frequency red shift ($(d(\Delta E_{disp})/dr_{OH})$ being negative throughout the complete range of investigated r_{OH} values). Such prevalence of the factors contributing to the O−H stretching frequency blue shift, which is partially suppressed only by the dispersion component, leads to the experimentally observed actual frequency blue shift when the H_2 tagging is realized from the charged side of protonated betaineH(+).

4. CONCLUSIONS

In the present paper, we have provided an in-depth analysis of the intermolecular interaction between protonated betaine and molecular hydrogen in the gas phase at IRMPD spectroscopic conditions, using state-of-the-art quantum chemical approaches. Our new insights shed some new light on the fundamental issues related to the wide diapason of intermolecular hydrogen bonds and the character of the proton acceptors. We investigate the performance of a wide range of DFT functionals for the calculation of anharmonic vibrational frequency shifts of the studied system, which are essential for the correct interpretation of the experimental IRMPD data. The main conclusions from this study may be summarized as follows.

- When the protonated betaine molecule is tagged with molecular hydrogen from the OH group side, it is the σ bond of molecular hydrogen that plays the role of hydrogen-bonding proton acceptor. The tagging thus induces a small yet significant red shift of the protonated betaine O−H stretching mode.
- To provide a good agreement between theory and experiment, anharmonic vibrational frequency shifts must be computed with specifically designed DFT functionals, such as Handy's group HCTH/407.
- Empirical dispersion correction of the functionals that lead to overestimated OH stretching frequency shifts enhances this systematic error due to further flattening of the OH stretching potential in the intermolecular region.
- A comparative analysis of the OH stretching potential with the full-wave function (i.e., Kohn−Sham) approach, charge field perturbation method, and NBO deletion analysis reveals that the intermolecular charge-transfer interaction governs the overall OH stretching frequency shift when betaineH(+) molecule is tagged with molecular hydrogen from the OH group side. This charge transfer occurs from the σ_{HH} orbital to the σ^*_{OH} orbital and governs the geometry of the interacting dimer as well, as the electrostatic dipole−quadrupole interaction energy term disfavors it.
- Bader analysis reveals the existence of a (3, −1) bond critical point between the OH group hydrogen atom of the protonated betaine and the middle of the H−H bond.
- The calculated $\rho(\vec{r}_c)$ value at this critical point is 0.008 au, while the $\nabla^2\rho(\vec{r}_c)$ value is 0.02557 au. Both the $\rho(\vec{r}_c)$ and the $\nabla^2\rho(\vec{r}_c)$ values at this critical point fall within the range defined as a basic criterion for the existence of hydrogen bonds, though the electron density Laplacian tends to be close to the lower limit.
- NCI analysis based on the reduced density gradient reveals that the sign$(\lambda_2)\cdot\rho$ value for the OH···H_2 contact is negative, which indicates the attractive character of

https://doi.org/10.1021/acs.jpca.4c01331
J. Phys. Chem. A 2024, 128, 3968−3981

this interaction. It is, however, weaker than the intramolecular attractive CH···O interactions.

- Second-generation ALMO-EDA 2 analysis of the O−H stretching vibrational potential allowed us to conclude that in the case of betaineH(+) tagged from the OH group side, the permanent electrostatics (ΔE_{elec}), polarization (ΔE_{pol}), and charge-transfer (ΔE_{ct}) contributions to the total intermolecular interaction energy favor the weak hydrogen bond formation and induce a small red shift of the fundamental O−H stretching frequency. The ΔE_{ct} term contributes most to the frequency red shift. Pauli repulsion interaction induces O−H stretching frequency blue shift, an effect which is a direct consequence of the confinement of the high-amplitude O−H stretching motion by the tagging molecule.

■ ASSOCIATED CONTENT

Supporting Information

The Supporting Information is available free of charge at https://pubs.acs.org/doi/10.1021/acs.jpca.4c01331.

Tables containing the complete theoretical results, including interaction energies and basis set superposition errors, harmonic and anharmonic vibrational frequency shifts, and the additional figure illustrating the agreement between computed and experimentally measured harmonic vibrational frequency shifts for the two minima on the studied potential energy surfaces (the OH-tagged and the charged side-tagged one) (PDF)

■ AUTHOR INFORMATION

Corresponding Author

Ljupcho Pejov − *Institute of Chemistry, Faculty of Natural Sciences and Mathematics, SS Cyril and Methodius University, 1000 Skopje, Republic of North Macedonia; Department of Chemistry, Bioscience and Environmental Engineering, Faculty of Science and Technology, University of Stavanger, 4036 Stavanger, Norway; The Polytechnic School, Ira A. Fulton Schools of Engineering, Arizona State University, Arizona 85212, United States;* orcid.org/0000-0002-0108-3413; Email: ljupcop@pmf.ukim.mk, ljupcho.pejov@asu.edu

Author

Blagoj Achevski − *Institute of Chemistry, Faculty of Natural Sciences and Mathematics, SS Cyril and Methodius University, 1000 Skopje, Republic of North Macedonia; Faculty of Pharmacy, SS Cyril and Methodius University, 1000 Skopje, Republic of North Macedonia;* orcid.org/0000-0003-2181-3134

Complete contact information is available at: https://pubs.acs.org/10.1021/acs.jpca.4c01331

Notes

The authors declare no competing financial interest.

■ REFERENCES

(1) Polfer, N. C. Infrared multiple photon dissociation spectroscopy of trapped ions. *Chem. Soc. Rev.* **2011**, *40*, 2211−2221.

(2) Okumura, M.; Yeh, L. I.; Myers, J. D.; Lee, Y. T. Infrared spectra of the cluster ions $H_7O_3^+ \cdot H_2$ and $H_9O_4^+ \cdot H_2$. *J. Chem. Phys.* **1986**, *85*, 2328−2329.

(3) Okimura, M.; Yeh, L. I.; Myers, J. D.; Lee, Y. T. Infrared spectra of the solvated hydronium ion: Vibrational predissociation spectroscopy of mass-selected $H_3O^+ \cdot (H_2O)_n \cdot (H_2)_m$. *J. Phys. Chem. A* **1990**, *94*, 3416−3427, DOI: 10.1021/j100372a014.

(4) Duncan, M. A. Frontiers in the spectroscopy of mass-selected molecular ions. *Int. J. Mass Spectrom.* **2000**, *200*, 545−569.

(5) Kamrath, M. Z.; Relph, R. A.; Guasco, T. L.; Leavitt, C. M.; Johnson, M. A. Vibrational predissociation spectroscopy of the H_2-tagged mono- and dicarboxylate anions of dodecanedioic acid. *Int. J. Mass Spectrom.* **2011**, *300*, 91−98.

(6) Kamrath, M. Z.; Garand, E.; Jordan, P. A.; Leavitt, C. M.; Wolk, A. B.; Van Stipdonk, M. J.; Miller, S. J.; Johnson, M. A. Vibrational characterization of simple peptides using cryogenic infrared photodissociation of H_2-tagged, mass-selected ions. *J. Am. Chem. Soc.* **2011**, *133*, 6440−6448.

(7) Masson, A.; Williams, E. R.; Rizzo, T. R. Molecular hydrogen messengers can lead to structural infidelity: A cautionary tale of protonated glycine. *J. Chem. Phys.* **2015**, *143*, No. 104313, DOI: 10.1063/1.4930196.

(8) Kocevski, V.; Pejov, L. Anharmonic vibrational frequency shifts upon interaction of phenol(+) with the open shell ligand O_2. The performance of DFT methods versus MP2. *J. Phys. Chem. A* **2012**, *116*, 1939−1949.

(9) Kocevski, V.; Pejov, L. On the assessment of some new meta-hybrid and generalized gradient approximation functionals for calculation of anharmonic vibrational frequency shifts in hydrogen-bonded dimers. *J. Phys. Chem. A* **2010**, *114*, 4354−4363.

(10) Wierzbicki, A.; Bowman, J. M. GVCSF: A general code to perform vibrational self-consistent field calculations. *Comput. Phys. Commun.* **1988**, *51*, 225−232.

(11) Carter, S.; Culi, S. J.; Bowman, J. M. Vibrational self-consistent field method for many-mode systems: A new approach and application to the vibrations of CO adsorbed on Cu(100). *J. Chem. Phys.* **1997**, *107*, 10458−10469.

(12) Bulik, I. W.; Frisch, M. J.; Vaccaro, P. H. Vibrational self-consistent field theory using optimized curvilinear coordinates. *J. Chem. Phys.* **2017**, *147*, No. 044110, DOI: 10.1063/1.4995440.

(13) Roy, T. K.; Gerber, R. B. Vibrational self-consistent field calculations for spectroscopy of biological molecules: new algorithmic developments and applications. *Phys. Chem. Chem. Phys.* **2013**, *15*, 9468−9492.

(14) Barone, V. Anharmonic vibrational properties by a fully automated second-order perturbative approach. *J. Chem. Phys.* **2005**, *122*, No. 014108.

(15) Silvi, B.; Wieczorek, R.; Latajka, Z.; Alikhani, M. E.; Dkhissi, A.; Bouteiller, Y. Critical analysis of the calculated frequency shifts of hydrogen-bonded complexes. *J. Chem. Phys.* **1999**, *111*, 6671−6678.

(16) Bader, R. F. W. *Atoms in Molecules: A Quantum Theory*; Oxford University Press: Oxford, U.K., 1990.

(17) Foster, J. P.; Weinhold, F. Natural hybrid orbitals. *J. Am. Chem. Soc.* **1980**, *102*, 7211−7218.

(18) Reed, A. E.; Weinhold, F.; Curtiss, L. A.; Pochatko, D. J. Natural bond orbital analysis of molecular interactions: Theoretical studies of binary complexes of HF, H_2O, NH_3, N_2, O_2, F_2, CO, and CO_2 with HF, H_2O, and NH_3. *J. Chem. Phys.* **1986**, *84*, 5687−5705.

(19) Contreras-García, J.; Johnson, E. R.; Keinan, S.; Chaudret, R.; Piquemal, J.-P.; Beratan, D. N.; Yang, W. NCIPLOT: A program for plotting noncovalent interaction regions. *J. Chem. Theory Comput.* **2011**, *7*, 625−632.

(20) Pejov, L. A gradient-corrected density functional study of indole self-association through N−H···π hydrogen bonding. *Chem. Phys. Lett.* **2001**, *339*, 269−278.

(21) Horn, P. R.; Mao, Y.; Head-Gordon, M. Probing non-covalent interactions with a second-generation energy decomposition analysis using absolutely localized molecular orbitals. *Phys. Chem. Chem. Phys.* **2016**, *18*, 23067−23079.

(22) Horn, P. R.; Mao, Y.; Head-Gordon, M. Defining the contributions of permanent electrostatics, Pauli repulsion, and

dispersion in density functional theory calculations of intermolecular interaction energies. *J. Chem. Phys.* **2016**, *144*, No. 114107.
(23) Schlegel, H. B. Optimization of equilibrium geometries and transition structures. *J. Comput. Chem.* **1982**, *3*, 214−218.
(24) Boys, S. F.; Bernardi, F. The calculation of small molecular interactions by the differences of separate total energies. Some procedures with reduced errors. *Mol. Phys.* **1970**, *19*, 553−566.
(25) Becke, A. D. Density-functional thermochemistry. III. The role of exact exchange. *J. Chem. Phys.* **1993**, *98*, 5648−5652.
(26) Lee, C.; Yang, W.; Parr, R. G. Development of Colle-Salvetti correlation-energy formula into a functional of the electron density. *Phys. Rev. B* **1988**, *37*, 785−789.
(27) Yanai, T.; Tew, D. P.; Handy, N. C. A new hybrid exchange-correlation functional using the Coulomb-attenuating method (CAM-B3LYP). *Chem. Phys. Lett.* **2004**, *393*, 51−57.
(28) Grimme, S.; Ehrlich, S.; Goerigk, L. Effect of the damping function in dispersion corrected density functional theory. *J. Comput. Chem.* **2011**, *32*, 1456−1465.
(29) Henderson, T. M.; Izmaylov, A. F.; Scalmani, G.; Scuseria, G. E. Can short-range hybrids describe long-range-dependent properties? *J. Chem. Phys.* **2009**, *131*, No. 044108.
(30) Vydrov, O. A.; Scuseria, G. E. Assessment of a long-range corrected hybrid functional. *J. Chem. Phys.* **2006**, *125*, No. 234109.
(31) Hamprecht, F. A.; Cohen, A.; Tozer, D. J.; Handy, N. C. Development and assessment of new exchange-correlation functionals. *J. Chem. Phys.* **1998**, *109*, 6264−6271.
(32) Boese, A. D.; Doltsinis, N. L.; Handy, N. C.; Sprik, M. New generalized gradient approximation functionals. *J. Chem. Phys.* **2000**, *112*, 1670−1678.
(33) Grimme, S. Semiempirical hybrid density functional with perturbative second-order correlation. *J. Chem. Phys.* **2006**, *124*, No. 034108.
(34) Schwabe, T.; Grimme, S. Double-hybrid density functionals with long-range dispersion corrections: higher accuracy and extended applicability. *Phys. Chem. Chem. Phys.* **2007**, *9*, 3397−3406.
(35) Schwabe, T.; Grimme, S. Towards chemical accuracy for the thermodynamics of large molecules: new hybrid density functionals including non-local correlation effects. *Phys. Chem. Chem. Phys.* **2006**, *8*, 4398−4401.
(36) Grimme, S.; Ehrlich, S.; Goerigk, L. Effect of damping function in dispersion corrected density functional theory. *J. Comput. Chem.* **2011**, *32*, 1456−1465.
(37) Møller, C.; Plesset, M. S. Note on an approximation treatment for many-electron systems. *Phys. Rev.* **1934**, *46*, 618−622.
(38) Kendall, R. A.; Dunning, T. H., Jr.; Harrison, R. J. Electron affinities of the first-row atoms revisited. Systematic basis sets and wave functions. *J. Chem. Phys.* **1992**, *96*, 6796−6806.
(39) Zheng, G.; Witek, H.; Bobadova-Parvanova, P.; Irle, S.; Musaev, D. G.; Prabhakar, R.; Morokuma, K.; Lundberg, M.; Elstner, M.; Kohler, C.; Frauenheim, T. Parameter calibration of transition-metal elements for the spin-polarized self-consistent-charge density-functional tight-binding (DFTB) method: Sc, Ti, Fe, Co, and Ni. *J. Chem. Theory Comput.* **2007**, *3*, 1349−1367.
(40) Xantheas, S. S. On the importance of the fragment relaxation energy terms in the estimation of the basis set superposition error correction to the intermolecular interaction energy. *J. Chem. Phys.* **1996**, *104*, 8821−8824, DOI: 10.1063/1.471605.
(41) Stone, A. *The Theory of Intermolecular Forces*, 2nd ed.; Oxford University Press: Oxford, 2013.
(42) Popelier, P. L. *Atoms in Molecules: An Introduction*; Prentice-Hall: London, 2000.
(43) Reed, A. E.; Curtiss, L. A.; Weinhold, F. Intermolecular interactions from a natural bond orbital, donor-acceptor viewpoint. *Chem. Rev.* **1988**, *88*, 899−926.

https://doi.org/10.1021/acs.jpca.4c01331
J. Phys. Chem. A 2024, 128, 3968−3981